



HAL
open science

Numerical simulation of steady-state mixed convection sodium flow experiments

A. Genty, C. Roy, C. Geffray

► **To cite this version:**

A. Genty, C. Roy, C. Geffray. Numerical simulation of steady-state mixed convection sodium flow experiments. Nuclear Engineering and Design, 2021, 381, pp.111363. 10.1016/j.nucengdes.2021.111363 . cea-04394433

HAL Id: cea-04394433

<https://cea.hal.science/cea-04394433>

Submitted on 22 Jul 2024

HAL is a multi-disciplinary open access archive for the deposit and dissemination of scientific research documents, whether they are published or not. The documents may come from teaching and research institutions in France or abroad, or from public or private research centers.

L'archive ouverte pluridisciplinaire **HAL**, est destinée au dépôt et à la diffusion de documents scientifiques de niveau recherche, publiés ou non, émanant des établissements d'enseignement et de recherche français ou étrangers, des laboratoires publics ou privés.



Distributed under a Creative Commons Attribution - NonCommercial 4.0 International License

Numerical simulation of steady-state mixed convection sodium flow experiments

A. Genty^{a,*}, C. Roy^a and C. Geffray^a

^aUniversité Paris-Saclay, CEA, Service de Thermo-hydraulique et de Mécanique des Fluides, F-91191, Gif-sur-Yvette, France

ARTICLE INFO

Keywords:
Sodium
Mixed convection
CFD
RANS
 $k - \epsilon$
TrioCFD

ABSTRACT

In the framework of the validation of the TrioCFD code for mixed convection and steady-state sodium flows, four experiments obtained using the SUPERCAVNA experimental equipment and involving Richardson numbers ranging from 0.13 to 4.21 are simulated. The TrioCFD numerical tool uses a RANS approach with a $k - \epsilon$ turbulence model including a buoyancy term and the computed results are in very good agreement with the experiments.

1. Introduction

Among the nuclear reactor concepts currently being studied around the world are the sodium-cooled fast reactors SFR (Bertrand *et al.*, 2019; Chai *et al.*, 2020; Yeom *et al.*, 2020; Yu *et al.*, 2020; Khan *et al.*, 2020). The main feature of this technology lies in its capacity to consume depleted uranium issued from the pressurized water reactor nuclear fuel cycle.

The thermal-hydraulic flow in this type of reactor could have the particularity of being stratified (Ieda *et al.*, 1990). That is to say that the sodium of the highest temperature could accumulate in the upper part of certain core structures and modify heat exchanges, notably in the event of a primary circuit shutdown or a significant reduction in flow (Tenchine *et al.*, 2012). The modification of heat exchanges could be accompanied by significant thermal gradients on the metal structures, which would be harmful to maintain the integrity of the mechanical properties of these elements.

For safety reasons, it is therefore necessary to avoid the appearance of thermal stratification of sodium and the robustness of the concepts studied with respect to this point is tested using numerical simulation tools. In order to be able to validate these numerical simulation tools and the mathematical models describing the thermal-hydraulic flow of sodium, a good numerical simulation of experimental results is a key point (Tenchine *et al.*, 2012).

In this paper, we will present numerical simulation using the TrioCFD Code developed at CEA (Calvin *et al.*, 2002) of experimental results of sodium flow with thermal stratification. The experimental results were obtained in the years 1980 at the CEA thanks to the experimental device SUPERCAVNA (Super Cavity Na) involving several cubic meters of sodium at 300°C (Vidil *et al.*, 1988).

2. The SUPERCAVNA experiments

2.1. The experimental setup

The SUPERCAVNA test section was used at the CEA in Grenoble in the early 1980s. Its purpose was to study sodium

temperature rises due to thermo-gravity stratification of the flow in areas of the reactor that may have low flow velocities (such as parts of the lower plenum) following an emergency shutdown (Vidil *et al.*, 1988) or a significant reduction in the secondary coolant flow system (Tenchine *et al.*, 2012). It is schematically composed (Cf. Figure 1) of the assembly of two parts. The first part consists of a parallelepipedal cavity with a metallic wall in which a sodium flow is imposed by injection at a temperature $T_{in}^{cav} \approx 250^\circ\text{C}$ on the upstream side of its base and by withdrawing from the opposite downstream side of the base (Vidil *et al.*, 1988). The second part consists of a metal-walled channel where sodium at a temperature $T_{in}^{cha} > T_{in}^{cav}$ is injected in order to heat the sodium from the cavity by its downstream vertical side.

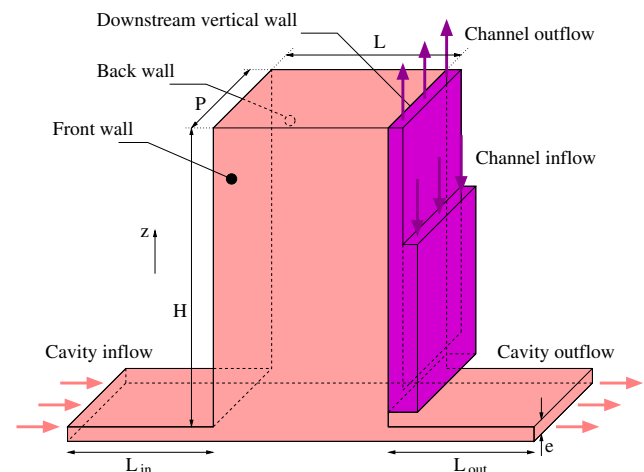


Figure 1: Simplified 3D diagram of the SUPERCAVNA test section.

In Figure 1, The sodium circulating in the cavity is represented in pink and the sodium circulating in the heating channel in purple. The operation of the test section is actually similar to that of a sodium / sodium heat exchanger with exchange through the vertical downstream sidewall. It should be noted that all sides of the experimental device shown in Figure 1 (with the exception of the inlets and outlets) are made of 6-mm-thick stainless steel plates. The main dimensions of the test section shown in Figure 1 are given in

*Corresponding author

alain.genty@cea.fr (A. Genty)

ORCID(s): 0000-0002-7009-3172 (A. Genty)

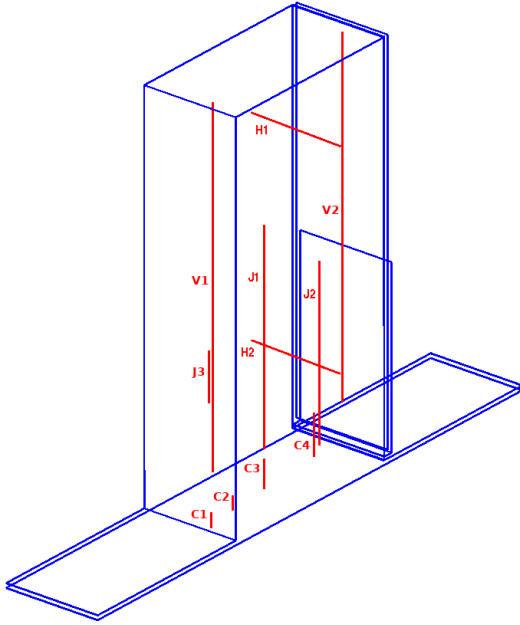
Table 1.

$L(m)$	$H(m)$	$P(m)$	$e(m)$	$L_{in}(m)$	$L_{out}(m)$
1.60	3.23	0.80	0.0304	1.50	1.50

Table 1

Geometric data of the SUPERCAVNA test section.

The experimental test section shown in Figure 1 was equipped with thermocouple lines in order to access the temperature field in the cavity. The position and denomination of these thermocouple lines can be seen in Figure 2. Note that since the objective of the experiments is to observe thermal stratification of the flow, the thermocouple lines are mainly placed vertically.

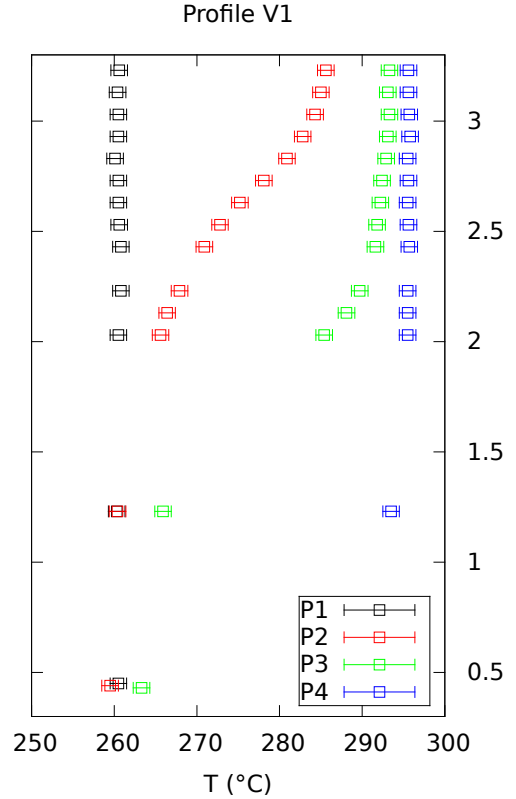

Figure 2: Temperature probes location in the cavity

Several dozen experiments were conducted during the test campaigns carried out on the SUPERCAVNA test section. These experiments consisted in studying the criteria for the appearance of steady state thermal stratification in the cavity by modulating the ratio between inlet flow rates into the cavity and in the heating channel. We will hereafter simulate four of these experiments.

2.2. Steady state experiments results

We have chosen to focus on SUPERCAVNA experiments $n^{\circ}90$, 22, 85 and 87, renamed hereafter $P1$, $P2$, $P3$ and $P4$ respectively for sake of clarity. This choice was based on the fact that these four experiments presented (or not) thermal stratification at different heights of the cavity as indicated in Figure 3 and are relevant of the whole thermal stratification

phenomena of concern varying from no thermal stratification to very strong thermal stratification.


Figure 3: Experimental temperature profile V1 for experiments $P1$, $P2$, $P3$ and $P4$.

It can be seen in Figure 3 that the $P1$ experiment does not present any thermal stratification. The three other experiments all exhibit stratification's at different heights. Indeed, experiment $P2$ present a stratification in the upper part of the cavity ($z \simeq 2.75 m$), experiment $P3$ present a stratification at mid-cavity height ($z \simeq 1.75 m$) and experiment $P4$ present a stratification in the lower part of the cavity ($z \simeq 0.75 m$).

As depicted previously, the position of the thermal stratification in the cavity was experimentally obtained by modulating the ratio between the inlet flow rates into the cavity and into the heating channel. The imposed mean velocities as well as inlet imposed temperatures defining the selected experiments are given in Table 2.

In Table 2, U_{in}^{cav} is the mean velocity inside the inlet cavity channel, U_{in}^{cha} is the mean velocity inside the heating inlet channel, T_{in}^{cav} is the imposed temperature at the entrance of the inlet cavity channel and T_{in}^{cha} is the imposed temperature at the entrance of the inlet heating channel.

For each experiment, we calculated the Reynolds number Re and the Richardson number Ri defined as (1) and (2)

$$Re = \frac{\rho U l}{\mu} \quad (1)$$

$$Ri = \frac{g \beta l \Delta T}{U^2} \quad (2)$$

Exp.	$U_{in}^{cav}(m.s^{-1})$	$U_{in}^{cha}(m.s^{-1})$	$T_{in}^{cav}(^{\circ}C)$	$T_{in}^{cha}(^{\circ}C)$
P1	1.721	0.811	252.2	303.3
P2	0.922	0.677	248.3	298.6
P3	0.678	0.747	250.4	299.1
P4	0.300	0.392	250.4	299.2

Table 2

Imposed velocities and temperatures values for P1, P2, P3 and P4 experiments

where ρ is the sodium density, U is the velocity, l is the characteristic length, μ is the dynamic viscosity, g is gravitational acceleration, β is the thermal expansion coefficient and ΔT represents the difference between the maximum and the minimum imposed temperatures. These values are given in Table 3.

Experiment	Re	Ri
P1	$1.29 \cdot 10^5$	0.13
P2	$0.69 \cdot 10^5$	0.46
P3	$0.51 \cdot 10^5$	0.82
P4	$0.22 \cdot 10^5$	4.21

Table 3

Non-dimensional numbers Re and Ri characterizing the experiments

Note that Re and Ri were calculated using the mean velocity inside the inlet cavity channel U_{in}^{cav} and Re was calculated using the characteristic length $l = e$ but Ri was calculated using $l = H$. Reynolds values given in Table 3 indicate that the flow is turbulent at the entrance of the cavity. We recall that the Richardson number Ri is the ratio between potential gravitational energy and kinetic energy or in other words represents the importance of natural convection relative to the forced convection. Flow regimes are considered as forced flow for $Ri < 0.3$, mixed flow for $0.3 < Ri < 16$ and natural convection for $Ri > 16$ (Sparrow *et al.*, 1959). The Richardson number values presented in Table 3 indicate that the selected experiments cover the flow range regimes from forced flow (P1) to mixed flow (P2 to P4). This dimensional study is in perfect agreement with the experimental results obtained with a flow P1 which does not present thermal stratification and flows P2 to P4 which present flows with increasingly marked thermal stratification with the increase of the Ri value.

3. Numerical simulation using TrioCFD

TrioCFD (formerly Trio_U) is a Computational Fluid Dynamic (CFD) code developed at CEA for many years (Calvin *et al.*, 2002; Tenchine *et al.*, 2012; Angeli *et al.*, 2017) and used to perform numerical simulations in many thermo-hydraulic applications in the nuclear field (Angeli, 2019; Bieder *et al.*, 2019).

3.1. Modelling approach

We seek to simulate the thermo-hydraulic behaviour of sodium, considered as an incompressible Newtonian fluid, by the numerical resolution of the system of equations including the Navier-Stokes equations (3) and the heat transport equation (4)

$$\begin{aligned} \vec{\nabla} \cdot \vec{u} &= 0 \\ \rho(\partial_t \vec{u} + \vec{\nabla} \cdot (\vec{u} \otimes \vec{u})) &= -\vec{\nabla} p + \mu \Delta \vec{u} + \rho \vec{g} \end{aligned} \quad (3)$$

$$\partial_t T + \vec{\nabla} \cdot (\vec{u} T) = \vec{\nabla} \cdot (\alpha \vec{\nabla} T) \quad (4)$$

with \vec{u} [$m \cdot s^{-1}$] the sodium velocity and p [$kg \cdot m^{-1} \cdot s^{-2}$] its pressure, the unknowns of the problem, ρ [$kg \cdot m^{-3}$] the density, μ [$kg \cdot m^{-1} \cdot s^{-1}$] the dynamic viscosity, $g = 9.81 m \cdot s^{-2}$ the acceleration of gravity, T [K] the sodium temperature and α [$m^2 \cdot s^{-1}$] its thermal diffusion coefficient defined by Equation (5)

$$\alpha = \frac{\lambda}{\rho C_p} \quad (5)$$

where λ [$kg \cdot m \cdot s^{-3} \cdot K^{-1}$] is the thermal conductivity of sodium and C_p [$m^2 \cdot s^{-2} \cdot K^{-1}$] its heat capacity.

We then chose to use a RANS (Reynolds-Averaged Navier-Stokes) approach. In this approach, the velocity \vec{u} is split into a mean velocity $\vec{\bar{u}} = \frac{1}{\tau} \int \vec{u}(\tau) d\tau$ and a fluctuating velocity \vec{u}' , the pressure is decomposed in the same way and a (Reynolds) averaging of system (3) is performed. An identical approach is applied to the heat equation (4).

The Boussinesq approximation for turbulence is then used to model the Reynolds stress tensor τ_{ij} in the form $\tau_{ij} = -\overline{u'_i u'_j} = \nu_t \left(\frac{\partial U_i}{\partial x_j} + \frac{\partial U_j}{\partial x_i} \right) - \frac{2}{3} k \delta_{ij}$ where ν_t is the turbulent kinematic viscosity, k is the turbulent kinetic energy and δ_{ij} is the Kronecker delta. Note that the term $\frac{2}{3} k \delta_{ij}$ is similar to a dynamic pressure stemming from the turbulence.

In addition, we have chosen to take into account the dependence of sodium density on temperature through the Boussinesq's approximation for density. Density is then considered constant in all terms of the Navier-Stokes equations except for the gravity term where it is assumed to vary linearly with temperature around a reference density ρ_{r0} and expressed mathematically by the relation (6)

$$\rho(T) = \rho_{r0}(1 - \beta(T - T_{r0})) \quad (6)$$

where ρ_{r0} is the density of sodium at the reference temperature T_{r0} and β the thermal expansion coefficient of sodium.

This approximation allows to rewrite the system of equation (3) in an identical way with the simple modification of the gravity term which then becomes temperature dependent. The global system combining flow and temperature equations is now coupled through of the said gravity term. It should be noted that Boussinesq's approximation (for density) can be considered valid for small density variations.

The thermal conditions encountered in the experiments verify that the term $\beta(T - T_{r0})$ is small in front of the unit and that $\Delta\rho/\rho$ is about one percent.

After taking the Reynolds averaging of the system composed of equations (3) and (4), using the the Boussinesq approximation for turbulence to express the Reynolds stress tensor and taking into account the Boussinesq approximation for the density, the final system of equations to be solved is written using Einstein notation

$$\frac{\partial U_i}{\partial x_i} = 0 \quad (7)$$

$$\frac{\partial U_i}{\partial t} + U_j \frac{\partial U_i}{\partial x_j} = -\frac{\partial P}{\partial x_i} + \frac{\partial}{\partial x_j} \left[(v + v_t) \left(\frac{\partial U_i}{\partial x_j} + \frac{\partial U_j}{\partial x_i} \right) \right] + (1 - \beta(T - T_0))g_i \quad (8)$$

$$\frac{\partial T}{\partial t} + U_j \frac{\partial T}{\partial x_j} = \frac{\partial}{\partial x_j} \left((\alpha + \alpha_t) \frac{\partial T}{\partial x_j} \right) \quad (9)$$

where U is the mean velocity, P the mean pressure divide by density ρ , T the mean temperature, $v = \frac{\mu}{\rho}$ the kinematic viscosity, v_t the turbulent kinematic viscosity, $\alpha = \frac{\lambda}{\rho C_p}$ the thermal diffusivity, $\alpha_t = \frac{v_t}{Pr_t}$ the turbulent thermal diffusivity of sodium where the turbulent Prandtl is set to the default value $Pr_t = 0.9$, μ is the dynamic viscosity, λ is the thermal conductivity and C_p is the heat capacity.

To be able to solve this system, we need to calculate the turbulent viscosity v_t introduced using the Boussinesq approximation for turbulence. To do so, we chose to use a variant of the $k - \epsilon$ standard model (Jones and Launder, 1972; Launder and Sharma, 1974; Launder and Spalding, 1974) introduced by Bahari and Hejazi (2009) in order to take into account buoyancy effects and defined by the set of equations (10)

$$\begin{aligned} v_t &= C_\mu \frac{k^2}{\epsilon} \\ \frac{\partial k}{\partial t} + \frac{\partial(U_j k)}{\partial x_j} &= \frac{\partial}{\partial x_j} \left[\left(v + \frac{v_t}{\sigma_k} \right) \frac{\partial k}{\partial x_j} \right] - \epsilon + P_k + G_k \\ \frac{\partial \epsilon}{\partial t} + \frac{\partial(U_j \epsilon)}{\partial x_j} &= \frac{\partial}{\partial x_j} \left[\left(v + \frac{v_t}{\sigma_\epsilon} \right) \frac{\partial \epsilon}{\partial x_j} \right] + C_{\epsilon 1} \frac{\epsilon}{k} P_k \\ &\quad - C_{\epsilon 2} \frac{\epsilon^2}{k} + C_{\epsilon 1} C_{\epsilon 3} G_k \frac{\epsilon}{k} \end{aligned} \quad (10)$$

where C_μ is a constant, k is the turbulent kinetic energy, ϵ is the rate of dissipation of turbulent kinetic energy, σ_k and σ_ϵ are Prandtl's numbers for k and ϵ respectively, $C_{\epsilon 1}$, $C_{\epsilon 2}$ and $C_{\epsilon 3}$ are constants, $P_k = \tau_{ij} \frac{\partial U_i}{\partial x_j}$ is the turbulent kinetic energy generation term and $G_k = \frac{v_t}{Pr_t} \beta g_i \nabla T$ is the production of turbulent kinetic energy related to buoyancy due to temperature gradients.

The value of the constants C_μ , $C_{\epsilon 1}$, $C_{\epsilon 2}$, $C_{\epsilon 3}$, σ_k and σ_ϵ are shown in Table 4 (Launder and Sharma, 1974; Bahari and Hejazi, 2009). Note that $C_{\epsilon 3}$ is set to zero in the case of unstable thermal stratification and is fixed to the unit in the stable case (Bahari and Hejazi, 2009).

The final system to solve is then composed of the mass conservation Equation (7), the momentum conservation Equa-

C_μ	$C_{\epsilon 1}$	$C_{\epsilon 2}$	$C_{\epsilon 3}$	σ_k	σ_ϵ
0.09	1.44	1.92	1.0	1.0	1.3

Table 4

Constants values used for the $k - \epsilon$ model

tion (8), the heat Equation (9) and the $k - \epsilon$ model including buoyancy effects system Equation (10).

In order to circumvent the excessive grid requirements needed to resolve the wall boundary sublayer, we used a law of the wall (Kalitzin *et al.*, 2005). We choose the general law of the wall proposed by Reichardt (1951) and described by Equation (11) which allow to calculate the velocity close to the walls

$$u^+ = \frac{1}{\kappa} \ln(1 + \kappa y^+) + 7.8 \left[1 - e^{-\frac{y^+}{11}} - \frac{y^+}{11} e^{-\frac{y^+}{3}} \right] \quad (11)$$

where $\kappa \simeq 0.41$ is the von Kármán constant, $u^+ = \frac{u}{u_\tau}$ is the dimensionless velocity, u_τ is the friction velocity and y^+ is the dimensionless wall distance. The Equation (11) considers that the velocity u^+ to compute is located inside the log layer of near-wall velocity profile and is then only valid for y^+ values in the range of ≈ 30 (Chen, 1973; Nagib *et al.*, 2007; George, 2007) to ≈ 300 (Cebeci, 2013). Note that the upper range for y^+ value for the log layer boundary increases with Reynolds number (Kalitzin *et al.*, 2005; Nagib *et al.*, 2007; George, 2007).

Assuming equilibrium conditions at the wall (production of turbulent kinetic energy is equal to dissipation of turbulent kinetic energy) we used the following boundary conditions for k and ϵ

$$k^+ = \frac{1}{\sqrt{C_\mu}} \quad (12)$$

with

$$k^+ = \frac{k}{u_\tau^2} \quad (13)$$

and

$$\epsilon^+ = \frac{C_\mu^{3/4}}{\kappa} \quad (14)$$

with

$$\epsilon^+ = \frac{\epsilon y_p}{k^{3/2}} \quad (15)$$

where y_p is the distance from the wall.

The walls of the SUPERCAVNA experimental device were made of steel and our thermal-hydraulics sodium problem is then coupled with heat transfer in solid. In order to take into account the heat transfer in the solid, the model is reduced for the solid part to heat Equation (9) where the velocity U and the turbulent thermal diffusivity α_t are set to zero and where the thermal diffusivity α is the one of the solid.

3.2. Numerics

The spatial discretization scheme used to solve Equations (7), (8), (9) and (10) is of the VDF (Finite Volume Difference) type on cartesian grid where pressure P and temperature T are computed at the center of the cells and velocities U are computed normal to the center of the edge cells through finite differences. This scheme is in fact similar to the Marker-and-Cell (MAC) method proposed by Harlow and Welch (1965).

The convective terms are discretized using a first order upwind scheme.

The time scheme used is an implicit Euler time scheme including a dynamic time step increment algorithm limited to 50 times the CFL condition. The convergence threshold of the implicit solver was set to 10^{-2} .

The solver used to solve the pressure system is of the Cholesky type.

It should be noted that the problem of fluid thermohydraulics and that of heat transfer in the solid are solved successively with a coupling through the heat flow crossing the fluid / solid interface. The heat flow is calculated by linear interpolation in order to ensure heat flux equality at the interface and no thermal wall law is used for the calculation of the heat flow in the fluid.

For further information, residuals of the solved equations (namely R_V for velocity, R_k for turbulent kinetic energy, R_ϵ for rate of dissipation of turbulent kinetic energy, R_{T_f} for fluid temperature and R_{T_s} for solid temperature) are given in Table 5 for each simulated experiment.

Exp.	R_V	R_k	R_ϵ	R_{T_f}	R_{T_s}
P1	4.5e-11	1.1e-12	1.4e-11	2.7e-09	2.6e-09
P2	6.7e-06	3.7e-08	1.8e-07	9.9e-05	8.9e-05
P3	6.4e-07	6.1e-09	6.3e-08	3.2e-05	4.2e-05
P4	6.8e-07	3.8e-09	6.8e-09	3.7e-04	9.3e-05

Table 5
Residuals of the solved equations for each experiment

3.3. The Mesh

We used the symmetry of the experimental device in y direction (see Figure 1) and only take into account half of the geometry in order to reduce the mesh size and the computation time.

The mesh was build in order to contain a dozen cells in the inlet and outlet sections of the cavity, as many as possible cells in the thickness of solid walls but with a size close to the size of fluid cells in contact with the walls and the size of fluid cells in contact with the wall that respect the validity of the wall law. The resulting mesh contains about 1 million rectangular parallelepipeds and a zoom on the bottom backside of the system is presented in Figure 4.

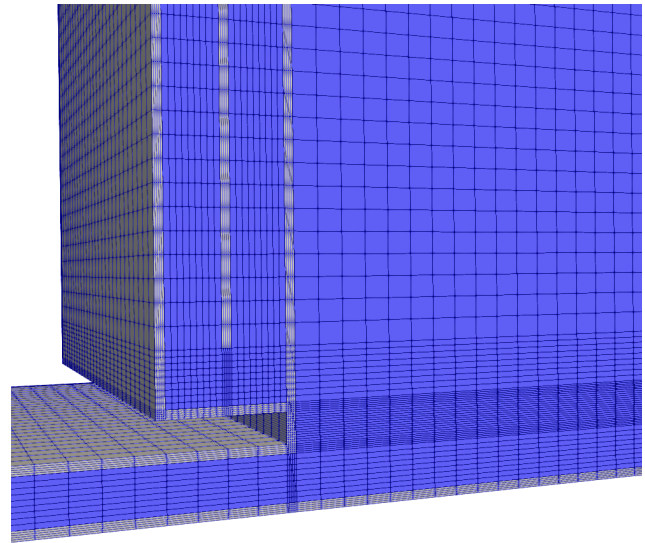


Figure 4: Zoom on the bottom backside of the mesh including outlet and heating sections. Fluid cells are drawn in blue and solid cells in grey

It should be noted that we have performed preliminary tests in 2D and 3D concerning the refinement of the mesh in order to ensure that the results obtained are not sensitive to the discretization in space. In 3D, we used three levels of discretization: a coarse mesh (about 150000 cells), the mesh presented previously in the article (about 1 million cells) and a much finer mesh (about 6 million cells) to simulate the P3 experiment. The results obtained are presented in Figure 5 for profile V1 with a temperature gap of less than 1°C for the two finer meshes. In view of the calculation time (several weeks of calculation) necessary to carry out the simulation of the P3 experiment with the finest mesh, we have chosen to present only the results obtained on the current mesh considered as "converged" and do not computed experiments P1, P2 and P4 with the finest mesh.

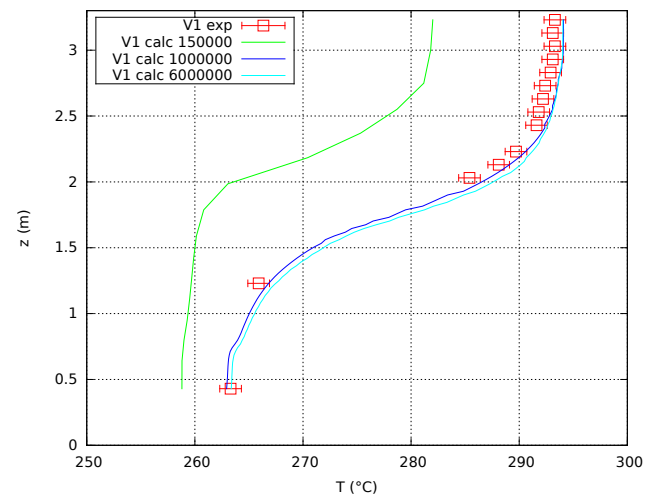


Figure 5: Sodium temperature profiles V1 for experiment P3 computed using several mesh refinements

3.4. Physical parameters

The sodium density ρ and its mass thermal capacity C_p are chosen constant and are given in Table 6 (Fink and Leibowitz, 1995).

ρ	C_p
885.5	1317.5

Table 6
Physical and thermal data of sodium at 275°C

We have chosen to consider dynamic viscosity μ , thermal conductivity λ and coefficient of thermal expansion β as linearly dependent on temperature and given by relations (16), (17) and (18), respectively (Fink and Leibowitz, 1995).

$$\mu = 5.8 \cdot 10^{-4} - 8 \cdot 10^{-7} T \quad (16)$$

$$\lambda = 94.4 - 0.064 T \quad (17)$$

$$\beta = 2.273 \cdot 10^{-4} + 10^{-7} T \quad (18)$$

The physical data of the steel are considered constant and are shown in Table 7.

ρ_{sol}	λ_{sol}	$C_{p_{sol}}$
8000	18	500

Table 7
Physical and thermal data of steel at 275°C

4. Steady state experiments simulations

The results of the TrioCFD computations performed to simulate the experiments $P1$, $P2$, $P3$ and $P4$ will be first presented in a qualitative way through thermal fields and in a second time through comparison to the available experimental temperature data.

4.1. Computed temperature fields

The steady-state sodium temperature fields computed with TrioCFD for experiments $P1$, $P2$, $P3$ and $P4$ are presented in Figures 6 and 7.

Figures 6 and 7 show that in steady-state the injected sodium through the left bottom cavity inflow undergoes a temperature increase as it rises along the downstream vertical wall in contact with the heating channel. We can retrieve on Figures 6 and 7 the qualitative behaviour observed experimentally on Figure 3 with the appearance (or not) of thermal stratification at different height of the cavity. Note that thermal stratifications are located between green (270°C) and yellow (280°C) colors. Thus, Figures 6a and 7a show that computed experiment $P1$ do not exhibit thermal stratification, Figures 6b and 7b indicate that the computed experiment $P2$ present a thermal stratification at a high height,

Figures 6c and 7c indicate that the computed experiment $P3$ present a thermal stratification at the mid-height of cavity as Figures 6d and 7d show that the computed experiment $P4$ present a thermal stratification at a low height in the cavity.

The computed current lines of the steady-state flow field colorized according to the temperature are presented for each experiment in Figure 8.

Figure 8 allows to observe the sodium circulation loops inside the cavity and thanks to the temperature coloring to locate the thermal stratification position. In this Figure, note that red color represent sodium temperature of about 300°C and blue color sodium temperature of about 250°C.

The computation of experiment $P1$ do not show any thermal stratification (See Figures 6a, 7a and 8a) and the sodium remains at a temperature close to the one of the injection of 250°C in the whole cavity with a sodium near the downstream heating wall slight increase as the sodium rises along this wall (See Figure 6a). The sodium flow circulation in the cavity remains high enough to dissipate this increase in temperature and is strong enough to drive a large and unique sodium flow loop inside the cavity (cf. Figure 8a).

The other three computed experiments (namely $P2$, $P3$ and $P4$) exhibit a thermal stratification at different height with a boundary corresponding to yellow color in Figures 6, 7 and 8. For these three computed experiments, the flow of sodium in the cavity can be schematized by three large flow loops. The first loop, of trigonometric orientation and triangular shape in deep blue in Figures 8b to 8d and in Figures 7b to 7d, is located at the bottom right of the cavity and sees the lowest temperature sodium circulating from the injection. This triangular loop is very high for $P2$ experiment computation and very flat for $P4$. The second flow loop, also triangular in shape but more convoluted with a global clockwise direction, is depicted in light blue to dark green colors in Figures 8b to 8d and correspond to the flow of sodium of medium temperature. As for the first loop, the second triangular loop is very high for $P2$ experiment computation and very flat for $P4$. The third loop is of rectangular shape and of very low intensity and is located in the upper part of the cavity. It is convoluted with a global clockwise direction and presents the highest temperatures. The thermal stratifications correspond to the boundary between the highest temperature circulation loop and the medium temperature sodium circulation loop (in yellow in Figures 8b to 8d).

4.2. Computed temperatures and data

In the following, the computed temperatures for experiments $P1$ to $P4$ will be compared to the experimental ones. The comparison will be performed by group of thermocouple lines shown in Figure 2.

Note that according to Vidil *et al.* (1988), the mean standard deviation σ of the measured temperatures in the SUPERCAVNA cavity is comprised between 0.5 and 3°C. We then chose to use the smallest observed one and to apply an uncertainty of $\pm 2\sigma = \pm 1^\circ\text{C}$ to the experimental temperatures data which gives a 95% probability that the real value

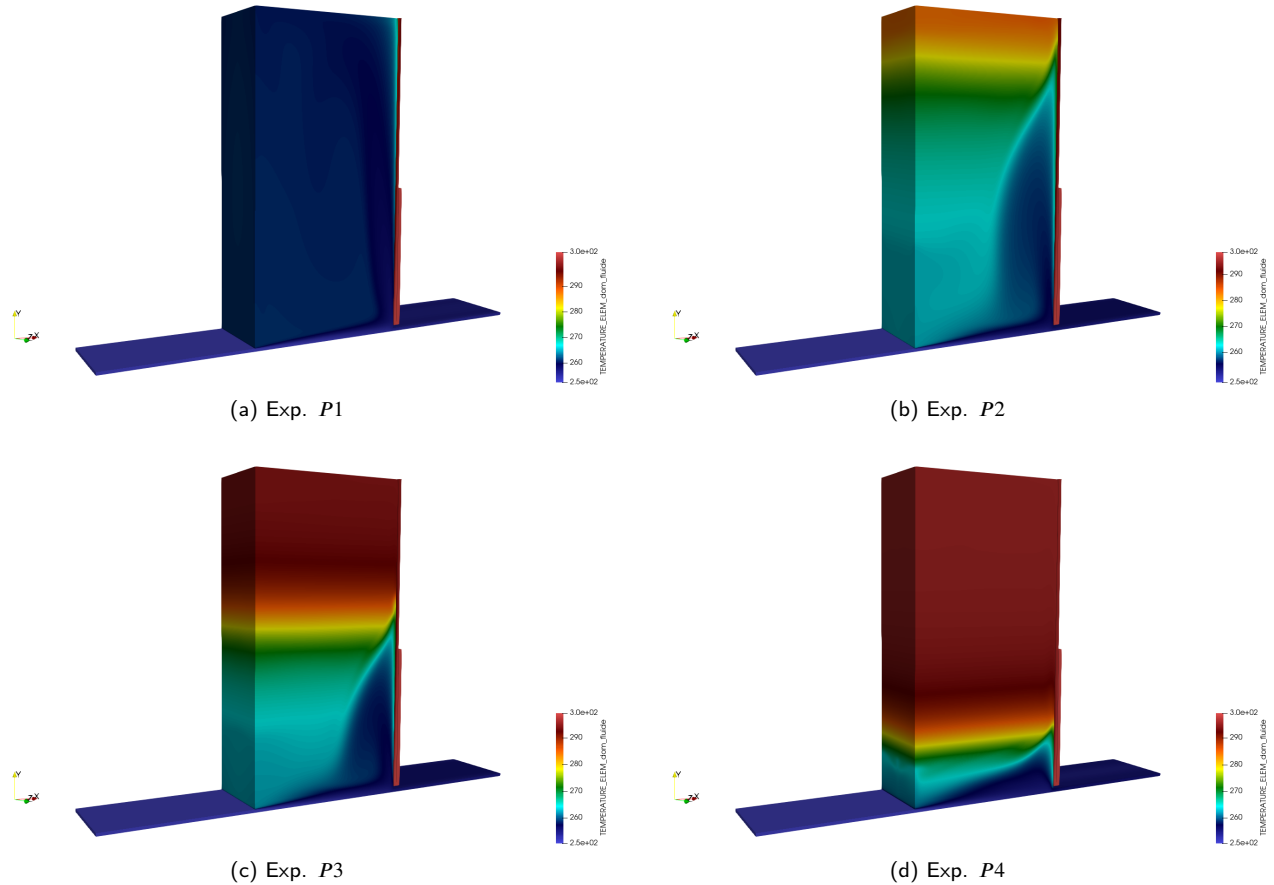


Figure 6: 3D temperature field of sodium

will be in this interval. All the experimental temperature data presented in the next Figures will then be plotted with a $\pm 1^\circ C$ error bar.

4.2.1. Profiles C

The thermocouple lines labeled "C" (namely C1, C2, C3 and C4) in Figure 2 are located vertically at an increasing distance from the cavity injection channel in the lower part of the cavity and allow to access to the evolution of the temperature in the shear layer of the entry jet. Figure 9 allow to compare, for thermocouple lines labeled "C", computed temperature profiles to experimental data for each experiment.

Figure 9 presents a good match between simulations and experimental data with a good simulation of the marked thermal gradients in this area. Note that 68% of the computed temperatures corresponding to a thermocouple position are included in the measurement uncertainty of $\pm 1^\circ C$, 90% have a deviation of less than $2^\circ C$ and the maximum deviation is of $4.4^\circ C$.

4.2.2. Profiles J

The thermocouple lines labeled "J" (namely J1, J2 and J3) in Figure 2 cover the central part of the cavity and allow to access to the temperature profile at the level of the

thermal stratification. Figure 10 allow to compare, for thermocouple lines labeled "J", computed temperature profiles to experimental data for each experiment. Note that data for experiment P2 are missing.

Figure 10 shows a fairly good match between simulations and experimental data and despite a greater gap than for profiles "C", the shape of the temperature profiles is well captured. Note that 90% of the calculated points have a deviation of less than $3.5^\circ C$ and the maximum deviation is of $4.2^\circ C$.

4.2.3. Profiles V

The thermocouple lines labeled "V" (namely V1 and V2) in Figure 2 are located vertically close to the left and right walls respectively and cover almost the entire height of the cavity and allow to access to the thermal stratification position. Figure 11 allow to compare, for thermocouple lines labeled "V", computed temperature profiles to experimental data for each experiment.

Figure 11 shows a really good match between simulations and experimental data with a precise simulation of the marked thermal gradients around the thermal stratification. Note that 67% of the computed temperatures are included in the data measurement uncertainty of $\pm 1^\circ C$, 89% have a deviation of less than $2^\circ C$ and the maximum deviation is of

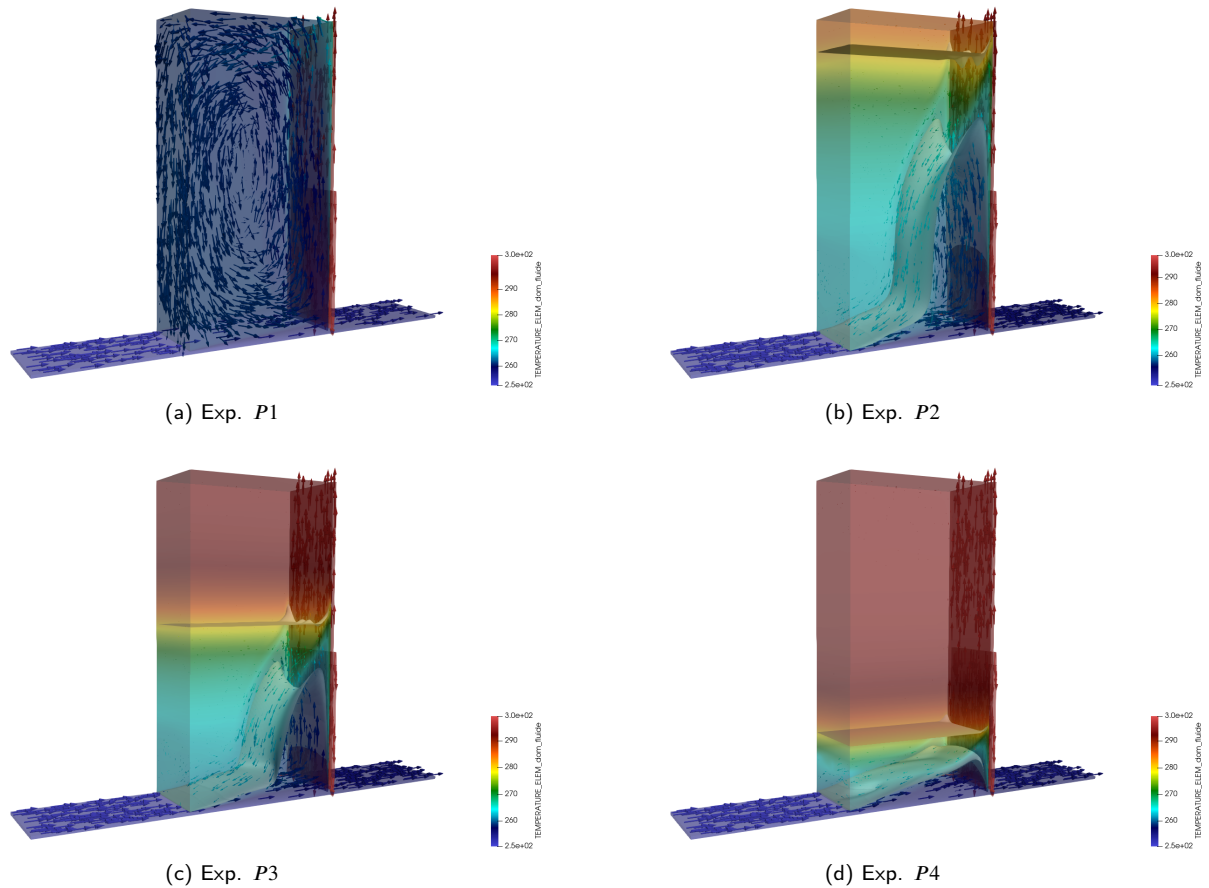


Figure 7: Semi-transparent 3D temperature field of sodium including velocity field and isotherm surface $T = 265^{\circ}\text{C}$ and $T = 280^{\circ}\text{C}$

3°C .

4.2.4. Profiles H

The thermocouple lines labeled "H" (namely $H1$ and $H2$) in Figure 2 are located horizontally close to the right wall of the cavity at two different height and allow to access to the transverse temperature profile inside the cavity. Unfortunately those data are only available for experiment $P2$ and Figure 12 allow to compare, for thermocouple lines labeled "H", computed temperature profiles to experimental data for experiment $P2$ only.

As can be seen in Figure 12, the computed profiles are well captured despite a too flat shape and the gap between the experimental data and the computations remains relatively small. Note that 70% of the computed points have a deviation of less than 2°C and the maximum temperature difference is 2.8°C .

4.2.5. Heating wall profile

An additional thermocouple line in the cavity is located vertically in a groove in the heating wall. As the thermocouples are welded to the wall, the measured temperatures are a mix between the temperature of the fluid and the temperature of the solid and represent the fluid/solid interface

temperature. The spatial discretization used to perform our computations does not allow to recover the temperature at the fluid/solid interface but at the centres of the mesh cells for fluid and for solid. We then chose to consider the average of the temperature of the solid mesh cells and of the fluid mesh cells on both side of the fluid/solid interface to be the temperature of the interface.

Figure 13 allow to compare, for the heating wall thermocouple line, averaged computed temperature profiles to experimental data for each experiment. Note that data for experiment $P1$ are missing.

Figure 13c exhibit a good match between simulations and experimental data despite the average approximation used to compute simulated wall surface temperature.

4.3. Synthesis

Comparisons of computed temperatures to experimental data performed in the previous section for experiments $P1$ to $P4$ indicate that our simulations are in good agreement with the experimental data. In order to quantify this agreement, we plot on Figure 14 the distribution histogram of the number of computed points within a given range of deviation from data values. Note that the number of data points over all experiments is of 522.

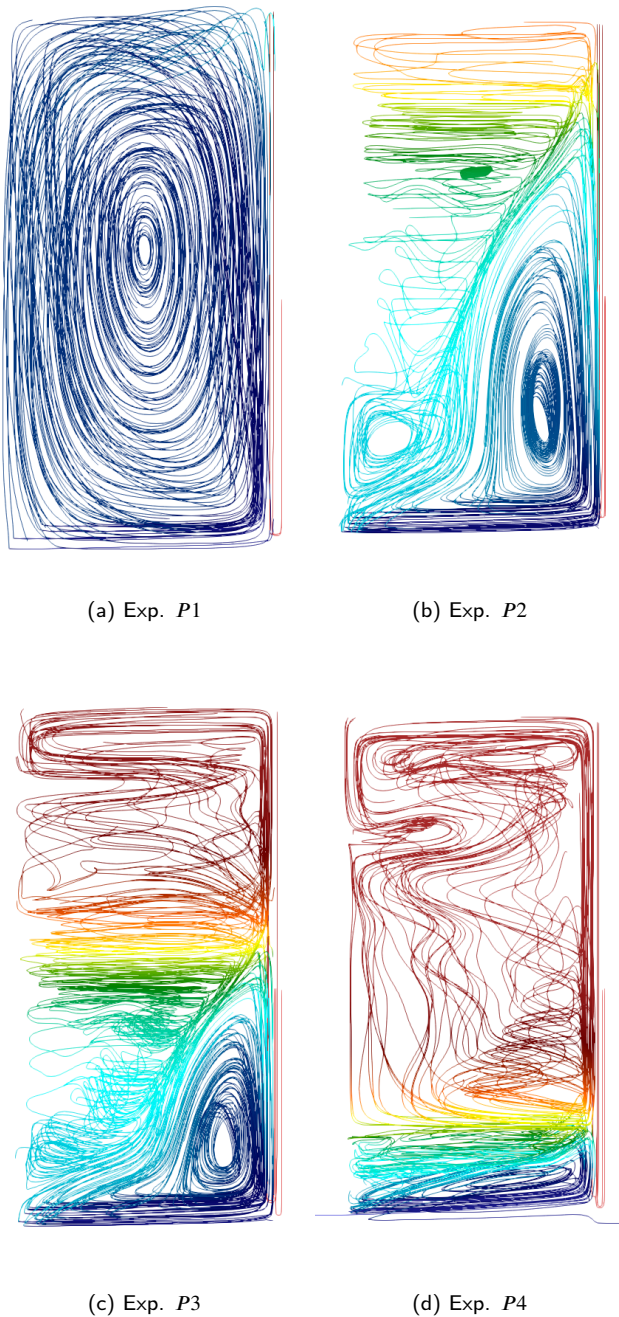


Figure 8: Current lines and temperature fields

The histogram presented in Figure 14 indicates that 55% of the computed temperatures points are within the measurement uncertainty interval ($\pm 1^\circ\text{C}$) and that 75% are computed with a gap to the experimental data lower than ($\pm 2^\circ\text{C}$).

5. Discussion

It should be noted that the simulation results presented here have been obtained using a very basic model both from the point of view of the $k - \varepsilon$ turbulence model and the turbulent thermal diffusion model used.

The $k - \varepsilon$ turbulence model modified to take into account the effects of buoyancy and using standard parameters values seems thus capable of recovering the flow with sufficient precision whereas it is known not to be well adapted to flows presenting in particular expansions and constrictions as in our case (Argyropoulos and Markatos, 2015). The use of more complex turbulence models could be carried out but without any real expected gain considering the results already obtained with the modified $k - \varepsilon$ model which seems sufficient in our case. In order to support this point, the P3 experiment was simulated using the $k - \omega$ SST turbulence model (Menter, 1993) available in Code_Saturne (<https://www.code-saturne.org/cms/>). The results obtained are presented in Appendix A and confirm the good results obtained using the $k - \varepsilon$ model.

The eddy thermal diffusion model used here, based on the Reynolds analogy, is also very simple and uses a thermal diffusivity coefficient $\alpha_t = \frac{\nu_t}{Pr_t}$ based on a constant turbulent Prandtl number set to 0.9 based on results obtained for water and air. It should be noted that more complex models of eddy thermal diffusivity taking into account tensor effects exist (Grötzbach, 2013; Kenjereš *et al.*, 2005; Otić and Grötzbach, 2007). Beyond the use of these models, the Pr_t set to 0.9 here is found higher in the case of low Reynolds liquid metal thermohydraulic flow with values of the order of 2 (Grötzbach, 2013) with a maximum limit of 2.6 (Bremhorst and Krebs, 1992) but strongly dependent on flow conditions such as velocity or Reynolds (Bremhorst and Krebs, 1992; Sheriff and O’Kane, 1981). It must be noted that for high Reynolds, Pr_t tends towards 0.9 (Sheriff and O’Kane, 1981; Kays, 1994) and that in our cavity the velocity field is highly variable suggesting that Pr_t is variable in space. Our model could therefore be improved by using a spatially variable Pr_t depending on the flow conditions as in the case of the model proposed by Kays (Kays, 1994) and given by relation (19)

$$Pr_t = 0.85 + 0.7 \frac{\alpha}{\nu_t} \quad (19)$$

It should be noted that in our case these model improvement can only be of second order in view of the good results already obtained. In order to verify our point of view, additional calculations were thus carried out in 2D (data not shown) using a Pr_t calculated from the Kays formula. The results obtained with the Kays formula are practically not modified with a maximum deviations lower than 1 degree.

The steady-state sodium turbulent kinetic energy and turbulent kinetic viscosity fields computed with TrioCFD for experiments P1, P2, P3 and P4 are presented in Figures 15 and 16. Note that in order to obtain a better view, only the half of the symmetric system (in y direction) is presented from the back side (heating section on the left side) using semi-transparency. The small impact of using Kay’s formula on the computed temperature fields is logical if one observes the turbulent viscosity fields presented in Figure 16 where turbulent viscosity values are much larger than sodium thermal diffusion $\alpha = 6.5 \cdot 10^{-5} \text{m}^2 \cdot \text{s}^{-1}$ in a large part of the domain and only of the same order of magnitude in

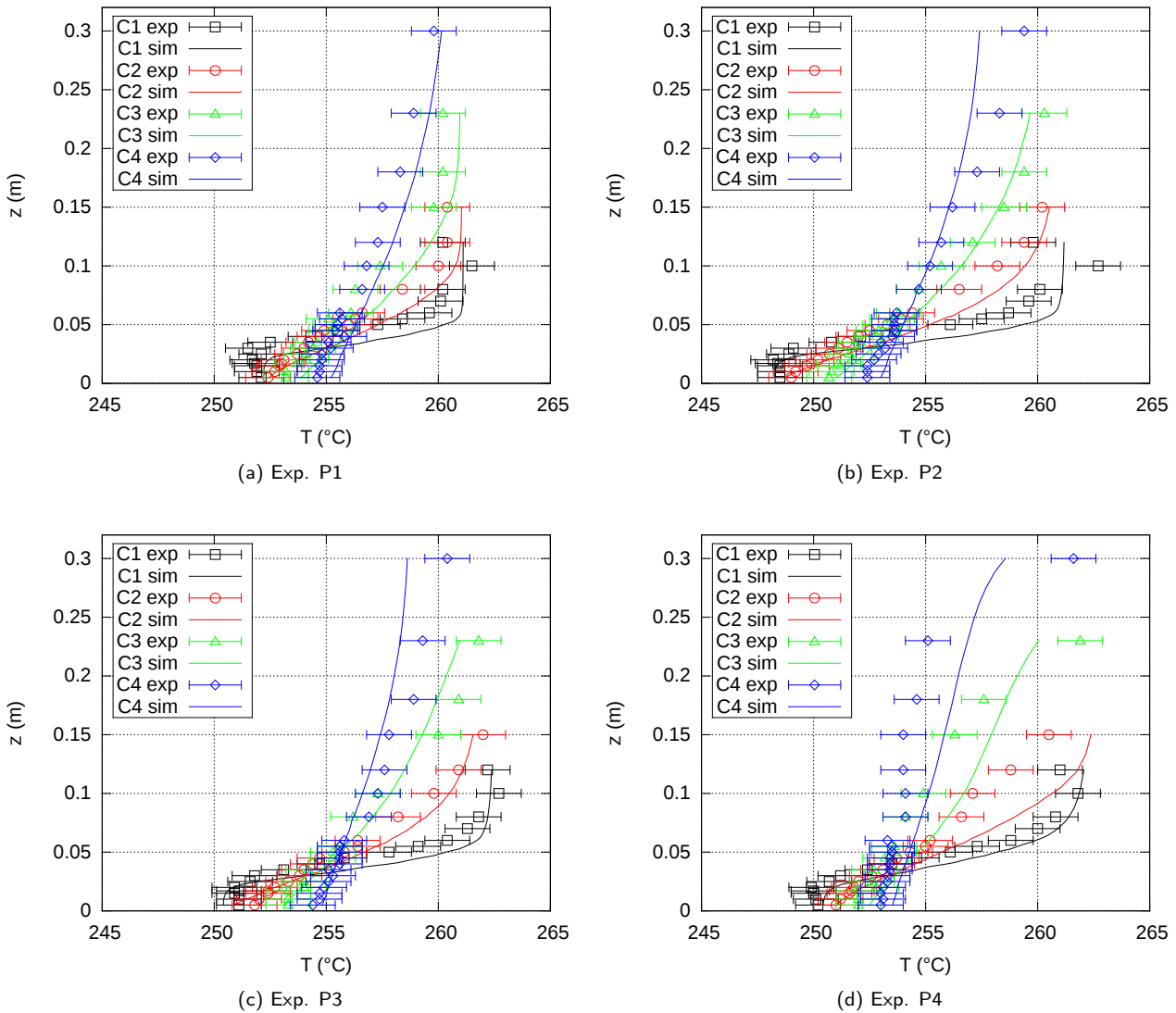


Figure 9: Computed temperature profiles (solid lines) and experimental data (markers) for the thermocouple lines labeled C1 to C4 and experiments P1 to P4

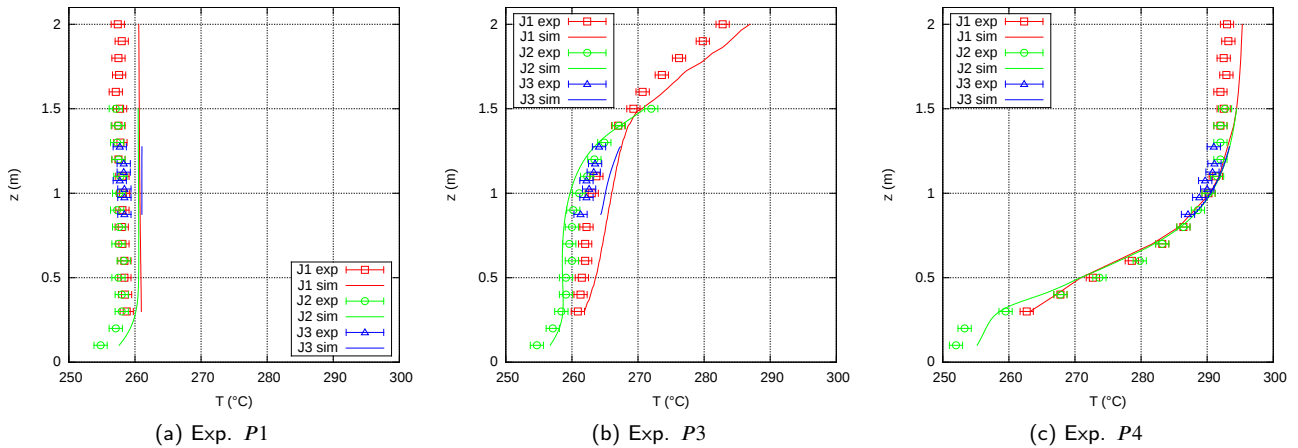


Figure 10: Computed temperature profiles (solid lines) and experimental data (markers) for the thermocouple lines labeled J1 to J3 and experiments P1, P3 and P4

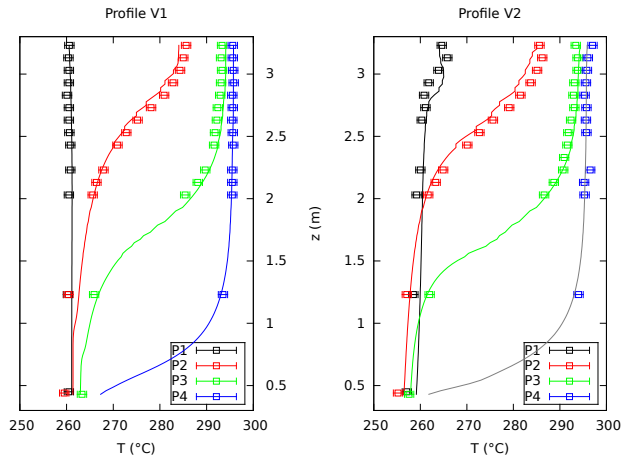


Figure 11: Computed temperature profiles (solid lines) and experimental data (markers) for the thermocouple lines $V1$ and $V2$ and experiments $P1$ to $P4$

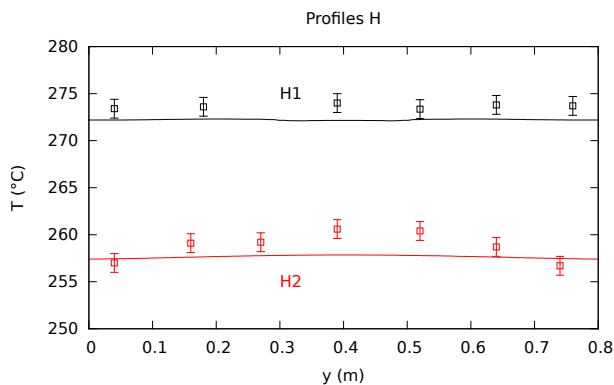


Figure 12: Computed temperature profiles (solid lines) and experimental data (markers) for the thermocouple lines $H1$ and $H2$ and experiments $P2$

part where temperature is almost constant and equal to the maximum temperature value of the field. Figures 15 and 16 also indicate that the increase of the stratification from experiment $P1$ to $P4$ (with a lower stratification line position) is strongly related to the lower turbulent diffusion at higher Ri numbers.

6. Conclusion

We performed four simulations of steady-state sodium mixed-convection experiments involving sodium obtained thanks to the SUPERCARVNA experimental device. These experimental results are typical of a wide range of mixed-convection flows varying from forced convection ($Ri = 0.13$) to mixed-convection with a very strong diffusive effect ($Ri = 4.21$).

We used a RANS approach implemented in the TrioCFD computational tool and, despite the fact that the $k - \epsilon$ turbulence model is not a priori well adapted to the simulation of these kind of experiments (Argyropoulos and Markatos, 2015), found a very good match between computed temper-

atures and experimental data. The numerical simulations allows, in particular, to perfectly recover the vertical temperature profiles and the position of the thermal stratification of the experiments and to validate the use of RANS approach to model steady-state thermohydraulic mixed-convection flows involving sodium in large cavities of similar form factor.

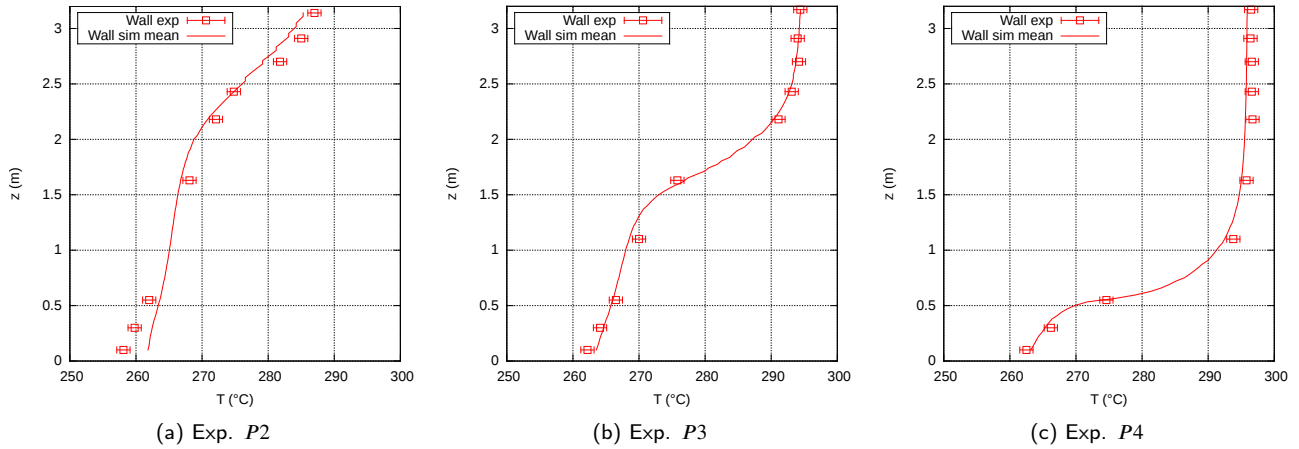


Figure 13: Computed averaged temperature profiles (solid lines) and experimental data (markers) for the heating wall thermocouple line and experiments $P2$, $P3$ and $P4$

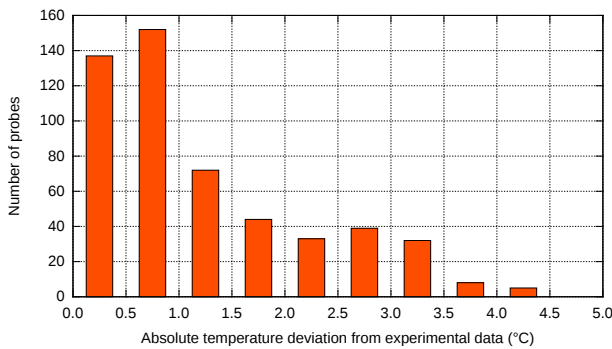


Figure 14: Number of computed points included in a given temperature deviation from data values

A. Computation of the P3 experiment using the $k-\omega$ SST turbulence model

Additional computation results for the P3 experiment using the $k-\omega$ SST turbulence model available in Code_Saturne (<https://www.code-saturne.org/cms/>) are presented here. The simulation of the P3 experiment was performed with the same mesh as the one used with TrioCFD and we also simulated the P3 experiment using the $k-\epsilon$ turbulence model of Code_Saturne for control.

The comparisons of the computed temperature profiles C , J and V with the experimental data are given in Figure 17.

As expected, from a global point of view, the use of a more complex turbulence model like the $k-\omega$ SST one does not improve the results obtained using the $k-\epsilon$ model.

A more detailed analysis of Figure 17 shows that the simulations performed with the $k-\epsilon$ model of TrioCFD and Code_Saturne give very close results. The temperature calculated with Code_Saturne is slightly higher with a maximum deviation of less than $0.5^\circ C$. The differences between the simulations obtained with the $k-\epsilon$ and $k-\omega$ SST mod-

els are more important, the $k-\omega$ SST model giving higher temperatures with a maximum difference of $3^\circ C$. The results obtained with the $k-\omega$ SST model are globally very slightly less accurate in the lower part of the cavity (0 - 0.1 m), slightly more accurate in the 0.1 - 0.3 m part and less accurate in the 0.5 - 2 m part.

From a more precise point of view, it can be considered that the $k-\omega$ SST model is less accurate due to the degradation of the J-profiles simulation by several degrees Celsius.

B. Data

For each temperature profile, the position of the probes, the experimentally measured temperature and the temperature calculated using TrioCFD for each experiment are given in the tables in this appendix.

The coordinates of the probes are given from an origin located in the lower left corner on the front side of the cavity. The right edge of the cavity is thus placed at $x = 1.6 m$, the back side at $y = 0.8 m$ and the roof at $z = 3.23 m$.

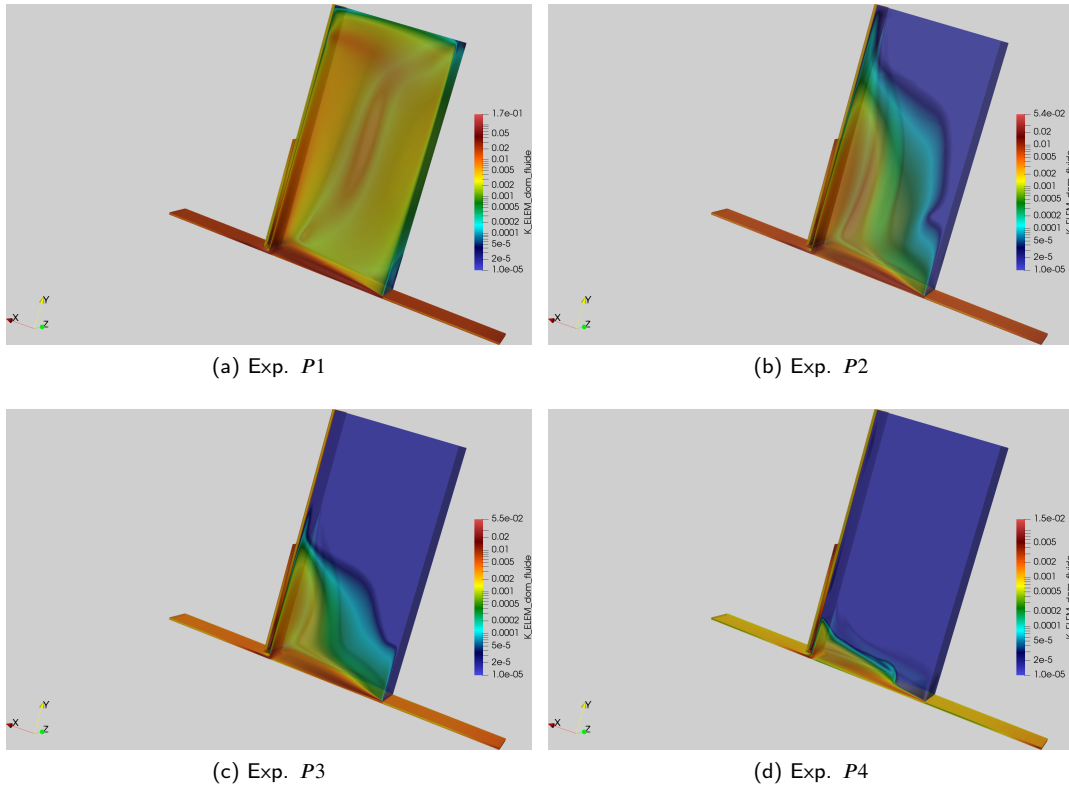


Figure 15: 3D turbulent kinetic energy field of sodium

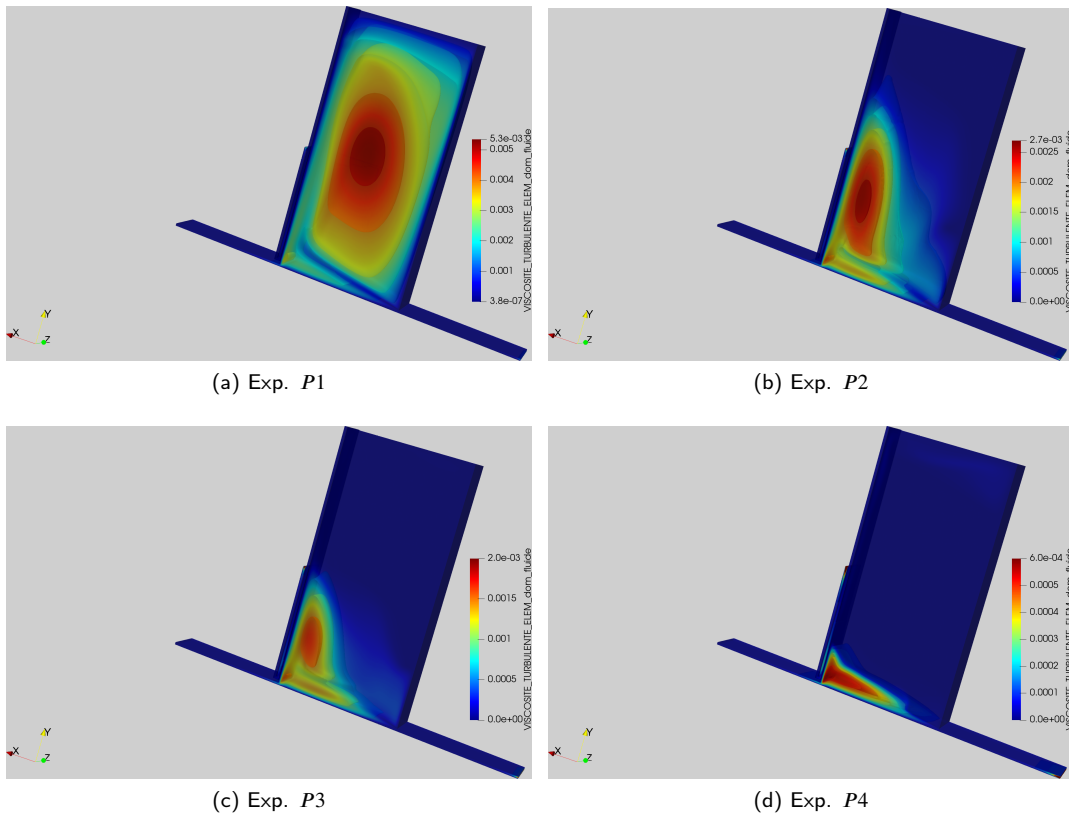


Figure 16: 3D turbulent kinetic viscosity field of sodium

probes location			P1		P2		P3		P4	
x	y	z	$T1_{exp}$	$T1_{calc}$	$T2_{exp}$	$T2_{calc}$	$T3_{exp}$	$T3_{calc}$	$T4_{exp}$	$T4_{calc}$
0.100	0.300	0.430	260.50	261.11	259.50	261.38	263.30	262.94	–	–
0.100	0.300	1.230	260.30	261.13	260.40	262.61	265.90	266.75	293.50	293.00
0.100	0.300	2.030	260.50	261.19	265.60	265.90	285.40	287.45	295.50	295.35
0.100	0.300	2.130	–	–	266.40	266.51	288.10	289.04	295.50	295.41
0.100	0.300	2.230	260.80	261.17	267.90	267.53	289.70	290.71	295.50	295.46
0.100	0.300	2.430	260.80	261.13	270.90	269.81	291.60	292.37	295.70	295.53
0.100	0.300	2.530	260.60	261.09	272.80	271.53	291.80	292.93	295.60	295.60
0.100	0.300	2.630	260.50	261.04	275.20	273.62	292.20	293.33	295.50	295.70
0.100	0.300	2.730	260.50	260.99	278.10	275.58	292.40	293.53	295.60	295.72
0.100	0.300	2.830	260.10	260.91	280.90	278.54	292.90	293.81	295.50	295.73
0.100	0.300	2.930	260.50	260.85	282.80	280.43	293.10	294.02	295.80	295.73
0.100	0.300	3.030	260.50	260.77	284.30	282.22	293.30	294.08	295.70	295.74
0.100	0.300	3.130	260.40	260.68	285.00	283.10	293.10	294.09	295.60	295.74
0.100	0.300	3.230	260.60	260.57	285.60	283.28	293.30	294.09	295.60	295.75

Table 8
Probes location, experimental and computed temperatures for profile V1

probes location			P1		P2		P3		P4	
x	y	z	$T1_{exp}$	$T1_{calc}$	$T2_{exp}$	$T2_{calc}$	$T3_{exp}$	$T3_{calc}$	$T4_{exp}$	$T4_{calc}$
1.500	0.500	0.430	257.10	259.16	255.20	256.50	257.60	257.89	–	–
1.500	0.500	1.230	258.50	259.97	257.10	257.77	262.00	261.39	294.00	293.00
1.500	0.500	2.030	259.20	260.49	261.70	261.45	286.60	287.50	295.30	295.33
1.500	0.500	2.130	–	–	263.30	262.30	288.70	289.08	295.20	295.38
1.500	0.500	2.230	260.00	260.64	264.90	263.85	290.70	290.73	296.50	295.47
1.500	0.500	2.330	–	–	–	–	290.90	291.66	–	–
1.500	0.500	2.430	–	–	270.10	267.44	291.60	292.38	–	–
1.500	0.500	2.530	–	–	272.70	270.41	291.80	292.92	295.70	295.61
1.500	0.500	2.630	260.30	261.25	275.60	273.98	292.40	293.34	295.60	295.64
1.500	0.500	2.730	261.10	261.56	279.10	275.66	293.10	293.57	295.70	295.65
1.500	0.500	2.830	260.80	263.07	281.50	278.77	292.90	293.82	295.30	295.67
1.500	0.500	2.930	261.80	264.72	283.70	280.51	293.10	293.91	295.60	295.68
1.500	0.500	3.030	263.90	265.00	285.10	281.84	293.80	293.98	295.80	295.70
1.500	0.500	3.130	265.80	264.39	286.20	282.80	293.80	294.08	296.00	295.75
1.500	0.500	3.230	264.60	264.11	285.60	284.39	293.40	294.29	297.00	295.85

Table 9
Probes location, experimental and computed temperatures for profile V2

References

- Argyropoulos, C. D., Markatos, N. C. 2015. Recent advances on the numerical modelling of turbulent flows. *Applied Mathematical Modelling*, 39, 693-732.
- Angeli, P.-E., Puscas, A., Fauchet, G., Cartalade, A. 2017. FVCA8 Benchmark for the Stokes and Navier-Stokes Equations with the TrioCFD Code - Benchmark Session. *Finite Volumes for Complex Applications VIII – Methods and Theoretical Aspects*, Springer, 181-203.
- Angeli, P.-E. 2019. Verification and validation of LES of a triple parallel jet flow in the context of a thermal striping investigation. *Nuclear Engineering and Design*, 353, 110210.
- Bahari, A. M., Hejazi, K. 2009. Investigation of buoyant parameters of $k - \epsilon$ turbulence model in gravity stratified flows. *International Journal of Physical and Mathematical Sciences*, 3(7), 494-501.
- Bertrand, F., Manchon, X., Marie, N., Droin, J.D., Schmitt, D., Lance, M., Sciora, P. 2019. Coupled thermalhydraulic-neutronic stability extended criterion in a SFR core. *Nuclear Engineering and Design*, 355, 110319.
- Bieder, U., Maillard, J., Gorsse, Y., Guenadou, D. 2019. CFD analysis of the flow in the MICAS experimental facility, a water model of the hot pool of a sodium cooled fast reactor. *Nuclear Engineering and Design*, 350, 67-77.
- Bremhorst, K., Krebs, L. 1992. Experimentally determined turbulent Prandtl number in liquid sodium at low Reynolds numbers. *International Journal of Heat and Mass Transfer*, 35(2), 351-359.
- Calvin, C., Cueto, O., Émonot, P. 2002. An object-oriented approach to the design of fluid mechanics software. *Mathematical Modelling and Numerical Analysis*, 36, 907-921.
- Chai, X., Zhao, L., Hu, W., Yang, Y., Liu, X., Xiong, J., Cheng, X. 2020. Numerical investigation of flow blockage accident in SFR fuel assembly. *Nuclear Engineering and Design*, 359, 110437.
- Chen, C. P. 1973. Détermination expérimentale du nombre de Prandtl turbulent près d'une paroi lisse. *Int. J. Mass. Transfer.*, 16, 1849-1862.
- Fink, J.K., Leibowitz, L. 1995. Thermodynamic and Transport Properties of Sodium Liquid and Vapor. Argonne National Laboratory, Report ANL/RE-95/2, 239 pages.
- George, W. K. 2007. Is there a universal log law for turbulent wall-bounded flow? *Phil. Trans. R. Soc. A*, 365, 786-806.
- Grötzbach, G. 2013. Challenges in low-Prandtl number heat transfer simulation and modelling. *Nuclear engineering and design*, 264, 41-55.
- Harlow, F. H., Welch, J. E. 1965. Numerical Calculation of Time-Dependent Viscous Incompressible Flow of Fluid with Free Surface.

probes location			P1		P2		P3		P4	
x	y	z	$T1_{exp}$	$T1_{calc}$	$T2_{exp}$	$T2_{calc}$	$T3_{exp}$	$T3_{calc}$	$T4_{exp}$	$T4_{calc}$
0.100	0.300	0.005	252.10	252.20	248.50	248.27	251.10	250.41	250.20	250.42
0.100	0.300	0.010	251.90	252.20	248.50	248.28	251.10	250.42	250.10	250.45
0.100	0.300	0.015	251.90	252.25	248.50	248.37	250.90	250.53	250.00	250.61
0.100	0.300	0.017	251.80	252.35	248.40	248.56	251.10	250.73	250.00	250.83
0.100	0.300	0.020	251.70	252.35	248.20	248.56	250.90	250.73	249.90	250.83
0.100	0.300	0.025	252.10	253.27	248.90	249.94	251.60	252.05	250.70	251.87
0.100	0.300	0.030	251.50	254.34	249.10	251.37	251.80	253.31	251.20	252.72
0.100	0.300	0.035	252.50	256.49	250.80	254.18	253.10	255.75	252.40	254.41
0.100	0.300	0.040	254.30	258.17	252.10	256.42	254.70	257.73	253.50	255.88
0.100	0.300	0.045	255.50	259.54	253.60	258.30	255.80	259.41	254.60	257.30
0.100	0.300	0.050	257.30	260.29	256.10	259.38	257.80	260.38	256.10	258.22
0.100	0.300	0.055	258.40	260.88	257.50	260.36	259.10	261.32	257.30	259.28
0.100	0.300	0.060	259.60	261.01	258.70	260.71	260.40	261.69	258.80	259.86
0.100	0.300	0.070	260.10	261.07	259.60	260.98	261.30	262.04	260.00	260.78
0.100	0.300	0.080	260.20	261.09	260.10	261.08	261.80	262.20	260.80	261.38
0.100	0.300	0.100	261.50	261.10	262.70	261.15	262.70	262.33	261.80	261.91
0.100	0.300	0.120	260.20	261.10	259.80	261.18	262.20	262.38	261.00	262.07

Table 10
Probes location, experimental and computed temperatures for profile C1

probes location			P1		P2		P3		P4	
x	y	z	$T1_{exp}$	$T1_{calc}$	$T2_{exp}$	$T2_{calc}$	$T3_{exp}$	$T3_{calc}$	$T4_{exp}$	$T4_{calc}$
0.400	0.350	0.005	252.40	252.45	249.00	248.76	251.80	250.96	251.00	251.02
0.400	0.350	0.010	252.70	252.67	249.20	249.09	252.00	251.28	251.20	251.20
0.400	0.350	0.015	252.90	253.29	249.70	249.96	252.40	252.07	251.60	251.74
0.400	0.350	0.017	253.00	253.66	249.90	250.47	252.40	252.53	251.70	252.08
0.400	0.350	0.020	253.10	253.66	250.20	250.47	252.70	252.54	251.80	252.09
0.400	0.350	0.025	253.70	254.47	250.70	251.54	253.30	253.48	252.00	252.82
0.400	0.350	0.030	254.00	254.88	251.10	252.09	253.80	253.96	252.60	253.21
0.400	0.350	0.035	254.20	255.60	251.50	253.02	254.00	254.78	253.10	253.92
0.400	0.350	0.040	254.70	256.24	252.00	253.84	254.40	255.50	253.50	254.56
0.400	0.350	0.045	254.90	256.88	252.50	254.66	254.70	256.23	253.70	255.25
0.400	0.350	0.050	256.00	257.35	253.30	255.24	255.80	256.73	254.30	255.75
0.400	0.350	0.055	256.30	257.92	253.90	255.95	256.40	257.37	255.00	256.42
0.400	0.350	0.060	256.60	258.28	254.40	256.38	256.40	257.75	255.20	256.84
0.400	0.350	0.080	258.40	259.88	256.50	258.27	258.20	259.44	256.60	258.96
0.400	0.350	0.100	260.00	260.86	258.20	259.63	259.80	260.67	257.10	261.01
0.400	0.350	0.120	260.40	260.98	259.40	260.04	260.90	261.05	258.80	261.74
0.400	0.350	0.150	260.40	261.04	260.20	260.53	262.00	261.55	260.50	262.38

Table 11
Probes location, experimental and computed temperatures for profile C2

Physics of Fluids, 8(12), 2182-2189.

Ieda, Y., Maekawa, I., Muramatsu, T., Nakanishi, S. 1990. Experimental and analytical studies of the thermal stratification phenomenon in the outlet plenum of fast breeder reactors. Nuclear engineering and design, 120(2-3), 403-414.

Jones, W. P., Launder, B. E. 1972. The prediction of laminarization with a two-equation model of turbulence. International Journal of Heat and Mass Transfer, 15, 301-314.

Kalitzin, G., Medic, G., Iaccarino, G., Durbin, P. 2005. Near-wall behavior of RANS turbulence models and implications for wall functions. Journal of Computational Physics, 204, 265-291.

Kays, W. M. 1994. Turbulent Prandtl number - where are we? Journal of Heat Transfer, 116(2), 284-295.

Kenjereš, S., Gunarjo, K. S., Hanjalić, K. 2005. Contribution to elliptic relaxation modelling of turbulent natural and mixed convection. International Journal of Heat and Fluid Flow, 26(4), 569-586.

Khan, F. U., Panchagnula, M. V., Velusamy, K. 2020. Experimental and computational investigations of gas entrainment in SFR due to rotation of partially submerged pump shaft. Annals of Nuclear Energy, 143, 107413.

Launder, B. E., Sharma, B.I. 1974. Application of the energy-dissipation model of turbulence to the calculation of flow near a spinning discs. Letters in Heat and Mass Transfer, 1, 131-138.

Launder, B. E., Spalding, D. B. 1974. The numerical computation of turbulence flows. Computer Methods in Applied Mechanics and Engineering, 1, 269-289.

Menter, F. R. 1993. Zonal Two Equation $k - \omega$ Turbulence Models For Aerodynamic Flow. American Institute of Aeronautics and Astronautics, AIAA 24th Fluid Dynamics Conference, July 6-9, Orlando, Florida, USA, Paper AIAA-93-2906.

probes location			P1		P2		P3		P4	
x	y	z	$T1_{exp}$	$T1_{calc}$	$T2_{exp}$	$T2_{calc}$	$T3_{exp}$	$T3_{calc}$	$T4_{exp}$	$T4_{calc}$
0.800	0.400	0.005	253.20	253.85	250.70	251.00	253.30	253.08	252.00	252.50
0.800	0.400	0.010	253.20	254.05	250.80	251.23	253.30	253.28	252.00	252.62
0.800	0.400	0.015	—	—	251.20	251.68	—	—	—	—
0.800	0.400	0.017	253.70	254.62	251.10	251.90	253.30	253.84	252.00	253.07
0.800	0.400	0.020	254.10	254.63	251.70	251.90	254.00	253.84	252.80	253.07
0.800	0.400	0.025	254.10	255.00	251.60	252.35	254.00	254.22	252.60	253.40
0.800	0.400	0.030	254.40	255.20	252.00	252.57	—	—	—	—
0.800	0.400	0.035	254.60	255.55	252.10	252.97	254.20	254.75	252.70	253.87
0.800	0.400	0.040	—	—	252.80	253.33	—	—	—	—
0.800	0.400	0.045	255.20	256.19	252.90	253.70	255.30	255.38	253.20	254.44
0.800	0.400	0.050	255.40	256.43	253.20	253.97	255.30	255.61	253.60	254.66
0.800	0.400	0.055	255.10	256.75	253.50	254.32	255.60	255.92	253.60	254.94
0.800	0.400	0.060	256.10	256.96	253.80	254.54	—	—	—	—
0.800	0.400	0.080	256.30	258.00	254.70	255.65	256.20	257.06	254.10	255.98
0.800	0.400	0.100	257.40	259.09	255.70	256.76	257.30	257.99	254.90	256.83
0.800	0.400	0.120	—	—	257.10	257.30	—	—	—	—
0.800	0.400	0.150	259.80	260.41	258.50	258.18	260.00	259.20	256.30	257.87
0.800	0.400	0.180	260.20	260.81	259.40	258.86	260.90	259.85	257.60	258.49
0.800	0.400	0.230	260.20	260.96	260.30	259.66	261.80	260.96	261.90	260.04

Table 12
Probes location, experimental and computed temperatures for profile C3

probes location			P1		P2		P3		P4	
x	y	z	$T1_{exp}$	$T1_{calc}$	$T2_{exp}$	$T2_{calc}$	$T3_{exp}$	$T3_{calc}$	$T4_{exp}$	$T4_{calc}$
1.400	0.450	0.005	254.60	255.21	252.40	253.00	254.40	254.82	253.00	253.53
1.400	0.450	0.010	254.70	255.31	252.40	253.08	254.70	254.88	253.10	253.58
1.400	0.450	0.015	254.70	255.47	252.40	253.22	254.70	255.00	253.00	253.68
1.400	0.450	0.020	254.80	255.55	252.70	253.29	254.90	255.06	253.10	253.73
1.400	0.450	0.025	254.80	255.71	252.90	253.43	255.10	255.18	253.30	253.84
1.400	0.450	0.030	255.20	255.79	253.20	253.51	255.30	255.24	253.30	253.90
1.400	0.450	0.035	255.10	255.93	253.00	253.64	255.10	255.35	253.40	254.00
1.400	0.450	0.040	255.80	256.06	253.50	253.76	255.60	255.45	253.40	254.09
1.400	0.450	0.045	255.40	256.20	253.60	253.90	255.60	255.57	253.40	254.20
1.400	0.450	0.050	255.50	256.31	253.60	254.00	255.60	255.65	253.50	254.27
1.400	0.450	0.055	255.70	256.46	253.60	254.13	255.60	255.76	253.50	254.38
1.400	0.450	0.060	255.60	256.55	253.70	254.22	255.80	255.83	253.30	254.44
1.400	0.450	0.080	256.60	257.05	254.70	254.69	256.90	256.23	254.10	254.80
1.400	0.450	0.100	256.80	257.64	255.20	255.23	257.30	256.70	254.10	255.21
1.400	0.450	0.120	257.30	257.93	255.70	255.51	257.60	256.94	254.00	255.42
1.400	0.450	0.150	257.50	258.46	256.20	256.01	257.80	257.38	254.00	255.80
1.400	0.450	0.180	258.30	258.92	257.30	256.43	258.90	257.76	254.60	256.16
1.400	0.450	0.230	258.90	259.62	258.30	257.04	259.30	258.31	255.10	256.90
1.400	0.450	0.300	259.80	260.14	259.40	257.41	260.40	258.62	261.60	258.55

Table 13
Probes location, experimental and computed temperatures for profile C4

Nagib, H. M., Chauhan, K. A., Monkewitz, P. A. 2007. Approach to an asymptotic state for zero pressure gradient turbulent boundary layers. *Phil. Trans. R. Soc. A*, 365, 755-770.

Otić, I. Grötzbach, G. 2007. Turbulent heat flux and temperature variance dissipation rate in natural convection in lead-bismuth. *Nuclear Science and Engineering*, 155(3), 489-496.

Reichardt, H. 1951. Vollständige Darstellung der turbulenten Geschwindigkeitsverteilung in glatten Leitungen. *Zeitschrift für Angewandte Mathematik und Mechanik*, 31(7), 208-219.

Sheriff, N., O’Kane, D. J. 1981. Sodium eddy diffusivity of heat measurements in a circular duct. *International Journal of Heat and Mass Transfer*, 34, 205-211.

Sparrow, E. M., Eichhorn, R., Gregg, J. L. 1959. Combined forced and free convection in a boundary layer flow. *Physics of Fluids*, 2(3), 319-328.

Cebeci, T. 2013. General behavior of turbulent boundary layers. *Analysis of turbulent flows with computer programs (Third Edition)*, Tuncer Cebeci (Ed.), Butterworth-Heinemann, 89-153.

Tenchine, D. 2010. Some thermal hydraulic challenges in sodium cooled fast reactors. *Nuclear Engineering and Design*, 240, 1195-1217.

Tenchine, D., Barthel, V., Bieder, U., Ducros, F., Fauchet, G., Fournier, C., Mathieu, B., Perdu, F., Quemere, P., Vandroux, S. 2012. Status of TRIO_U code for sodium cooled fast reactors. *Nuclear Engineering and*

probes location			P1		P2		P3		P4	
x	y	z	$T1_{exp}$	$T1_{calc}$	$T2_{exp}$	$T2_{calc}$	$T3_{exp}$	$T3_{calc}$	$T4_{exp}$	$T4_{calc}$
0.800	0.400	0.300	258.75	260.96	–	–	260.90	261.90	262.70	263.21
0.800	0.400	0.400	258.50	260.93	–	–	261.30	262.85	267.80	267.16
0.800	0.400	0.500	258.40	260.90	–	–	261.50	263.60	272.70	270.89
0.800	0.400	0.600	258.40	260.87	–	–	262.00	264.16	278.60	276.30
0.800	0.400	0.700	258.10	260.83	–	–	262.00	264.64	283.20	281.69
0.800	0.400	0.800	258.00	260.80	–	–	262.20	265.10	286.40	285.71
0.800	0.400	0.900	258.10	260.77	–	–	–	–	–	–
0.800	0.400	1.000	258.20	260.75	–	–	263.00	266.02	290.20	290.44
0.800	0.400	1.100	258.10	260.72	–	–	263.70	266.50	291.30	291.80
0.800	0.400	1.200	257.50	260.70	–	–	–	–	–	–
0.800	0.400	1.300	257.80	260.68	–	–	–	–	–	–
0.800	0.400	1.400	257.50	260.67	–	–	267.00	268.50	292.00	294.01
0.800	0.400	1.500	257.75	260.65	–	–	269.30	270.65	292.50	294.45
0.800	0.400	1.600	257.10	260.64	–	–	270.70	274.01	292.00	294.72
0.800	0.400	1.700	257.60	260.62	–	–	273.60	276.59	292.90	294.92
0.800	0.400	1.800	257.50	260.61	–	–	276.20	280.44	292.50	295.08
0.800	0.400	1.900	258.00	260.59	–	–	279.80	283.52	293.20	295.20
0.800	0.400	2.000	257.40	260.57	–	–	282.80	286.91	293.00	295.31

Table 14
Probes location, experimental and computed temperatures for profile J1

probes location			P1		P2		P3		P4	
x	y	z	$T1_{exp}$	$T1_{calc}$	$T2_{exp}$	$T2_{calc}$	$T3_{exp}$	$T3_{calc}$	$T4_{exp}$	$T4_{calc}$
1.400	0.400	0.100	254.80	257.61	–	–	254.70	256.71	252.00	255.20
1.400	0.400	0.200	257.10	259.27	–	–	257.10	258.08	253.30	256.51
1.400	0.400	0.300	258.00	260.13	–	–	258.40	258.63	259.50	258.53
1.400	0.400	0.400	258.00	260.46	–	–	259.10	258.66	267.80	264.71
1.400	0.400	0.500	257.50	260.55	–	–	259.10	258.59	273.70	270.61
1.400	0.400	0.600	258.30	260.57	–	–	260.00	258.54	279.80	276.41
1.400	0.400	0.700	257.50	260.57	–	–	259.60	258.59	283.20	281.69
1.400	0.400	0.800	257.60	260.56	–	–	260.00	258.77	286.40	285.71
1.400	0.400	0.900	257.30	260.55	–	–	260.20	259.11	288.60	288.51
1.400	0.400	1.000	257.60	260.54	–	–	261.10	259.65	290.20	290.44
1.400	0.400	1.100	257.80	260.53	–	–	262.30	260.47	291.50	291.80
1.400	0.400	1.200	257.50	260.52	–	–	263.40	261.73	292.00	292.77
1.400	0.400	1.300	257.30	260.51	–	–	264.90	263.70	292.00	293.48
1.400	0.400	1.400	257.40	260.50	–	–	267.10	266.78	292.00	294.01
1.400	0.400	1.500	257.10	260.48	–	–	272.00	271.01	292.70	294.45

Table 15
Probes location, experimental and computed temperatures for profile J2

Design, 242, 307-315.

Vidil, R., Grand, D., Leroux, F. 1988. Interaction of recirculation and stable stratification in a rectangular cavity filled with sodium. Nuclear Engineering and Design, 105, 321-332.

Yeom, S., Han, J.-W., Ryu, S., Kim, D., Eoh, J.-H., Choi, S.-R. 2020. Design and evaluation of reactor vault cooling system in PGSFR. Nuclear Engineering and Design, 365, 110717.

Yu, Y., Shemon, E.R., Kim, T.K., Merzari, E. 2020. Evaluation of hot channel factor for sodium-cooled fast reactors with multi-physics toolkit. Nuclear Engineering and Design, 365, 110704.

probes location			P1		P2		P3		P4	
x	y	z	$T1_{exp}$	$T1_{calc}$	$T2_{exp}$	$T2_{calc}$	$T3_{exp}$	$T3_{calc}$	$T4_{exp}$	$T4_{calc}$
0.200	0.400	0.875	258.40	261.04	–	–	261.30	264.37	287.10	287.81
0.200	0.400	0.975	258.40	261.04	–	–	262.20	264.90	288.80	289.96
0.200	0.400	1.025	258.40	261.04	–	–	262.60	265.19	290.00	290.88
0.200	0.400	1.075	257.70	261.04	–	–	262.20	265.54	289.70	291.63
0.200	0.400	1.125	258.30	261.05	–	–	263.30	265.86	290.80	292.11
0.200	0.400	1.175	258.30	261.05	–	–	263.50	266.34	291.10	292.65
0.200	0.400	1.275	257.70	261.05	–	–	264.10	267.32	291.00	293.39

Table 16
Probes location, experimental and computed temperatures for profile J3

probes location			P1		P2		P3		P4	
x	y	z	$T1_{exp}$	$T1_{calc}$	$T2_{exp}$	$T2_{calc}$	$T3_{exp}$	$T3_{calc}$	$T4_{exp}$	$T4_{calc}$
1.225	0.040	2.570	–	–	273.40	272.20	–	–	–	–
1.225	0.180	2.570	–	–	273.60	272.30	–	–	–	–
1.225	0.390	2.570	–	–	274.00	272.16	–	–	–	–
1.225	0.520	2.570	–	–	273.35	272.27	–	–	–	–
1.225	0.640	2.570	–	–	273.80	272.29	–	–	–	–
1.225	0.760	2.570	–	–	273.70	272.20	–	–	–	–

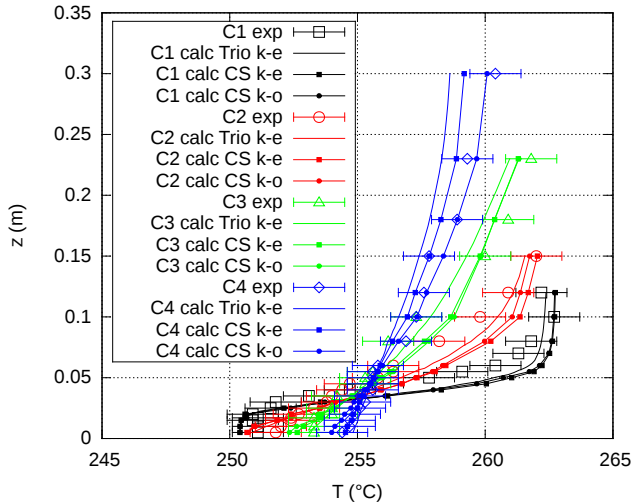
Table 17
Probes location, experimental and computed temperatures for profile H1

probes location			P1		P2		P3		P4	
x	y	z	$T1_{exp}$	$T1_{calc}$	$T2_{exp}$	$T2_{calc}$	$T3_{exp}$	$T3_{calc}$	$T4_{exp}$	$T4_{calc}$
1.225	0.040	0.818	–	–	257.00	257.44	–	–	–	–
1.225	0.160	0.818	–	–	259.10	257.61	–	–	–	–
1.225	0.270	0.818	–	–	259.20	257.78	–	–	–	–
1.225	0.390	0.818	–	–	260.60	257.85	–	–	–	–
1.225	0.520	0.818	–	–	260.40	257.78	–	–	–	–
1.225	0.640	0.818	–	–	258.70	257.61	–	–	–	–
1.225	0.740	0.818	–	–	256.70	257.48	–	–	–	–

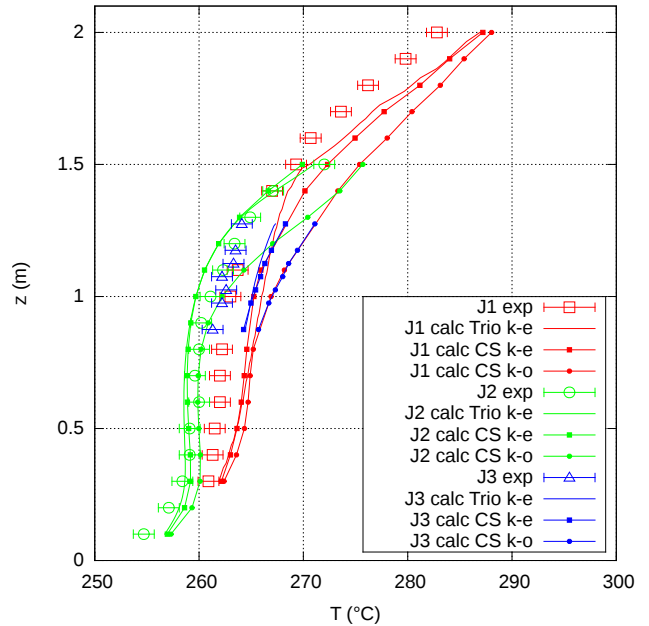
Table 18
Probes location, experimental and computed temperatures for profile H2

probes location			P1		P2		P3		P4	
x	y	z	$T1_{exp}$	$T1_{calc}$	$T2_{exp}$	$T2_{calc}$	$T3_{exp}$	$T3_{calc}$	$T4_{exp}$	$T4_{calc}$
1.600	0.400	0.100	–	–	258.10	261.81	262.20	263.53	262.50	263.16
1.600	0.400	0.300	–	–	259.80	262.45	264.10	264.64	266.20	265.35
1.600	0.400	0.550	–	–	262.00	263.60	266.50	266.01	274.60	274.50
1.600	0.400	1.100	–	–	–	–	270.00	268.52	293.80	292.50
1.600	0.400	1.630	–	–	268.10	266.76	275.80	277.02	295.80	295.02
1.600	0.400	2.180	–	–	272.10	270.90	291.10	290.42	296.70	295.62
1.600	0.400	2.430	–	–	274.80	274.88	293.10	292.76	296.60	295.74
1.600	0.400	2.700	–	–	281.80	279.10	294.20	293.76	296.60	295.82
1.600	0.400	2.910	–	–	285.00	282.80	294.00	294.15	296.40	295.85
1.600	0.400	3.170	–	–	287.00	285.29	294.40	294.41	296.50	295.90

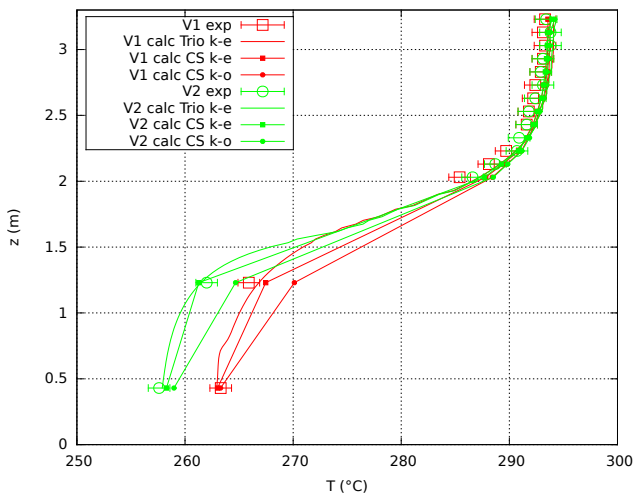
Table 19
Probes location, experimental and computed temperatures for heating wall profile



(a) Profiles C



(b) Profiles J



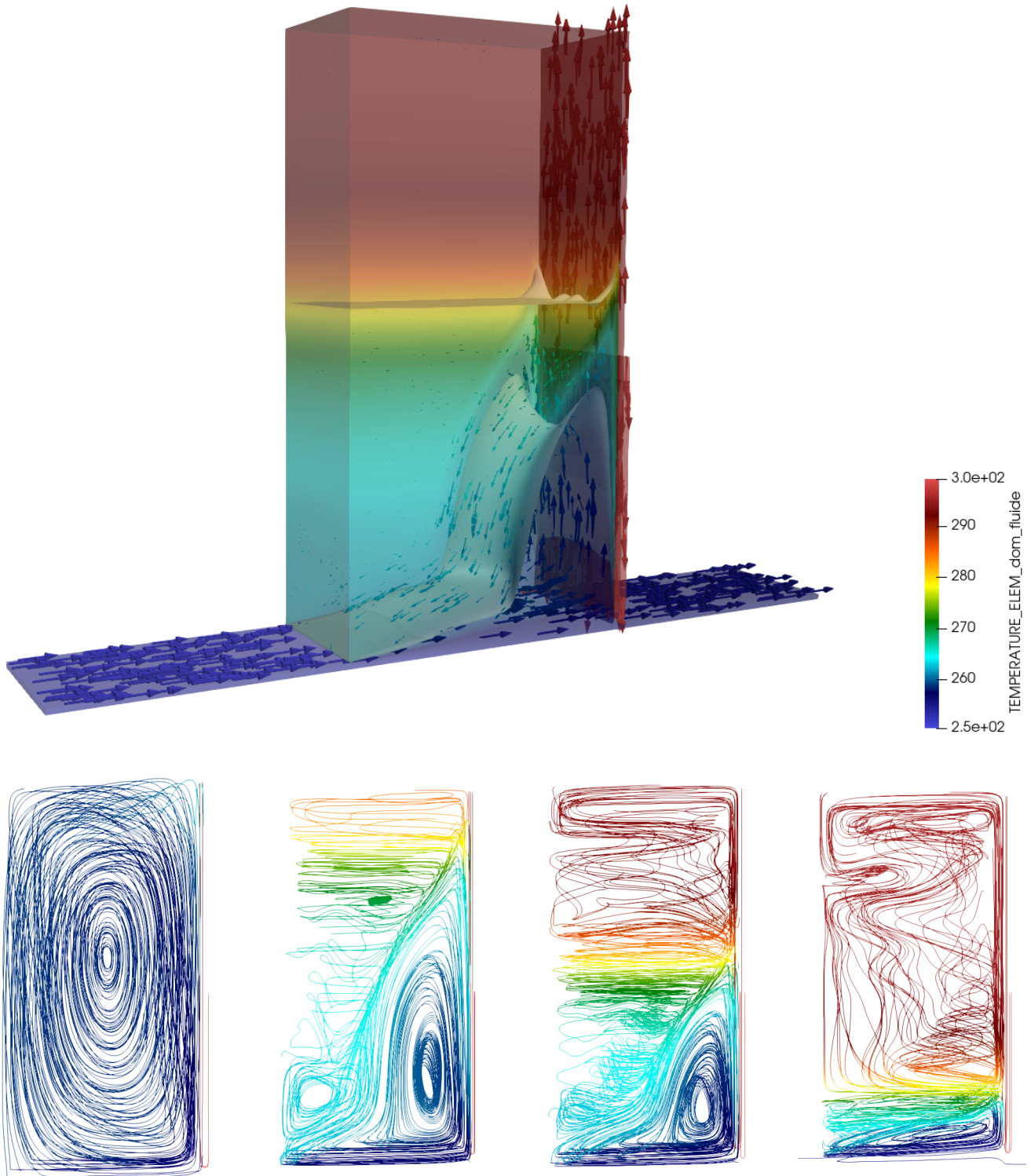
(c) Profiles V

Figure 17: Sodium temperature profiles for experiment P3 computed using $k-\epsilon$ (TrioCFD and Code_Saturne) and $k-\omega$ SST (Code_Saturne) models

Graphical Abstract

Numerical simulation of steady-state mixed convection sodium flow experiments

A. Genty, C. Roy, C. Geffray



Highlights

Numerical simulation of steady-state mixed convection sodium flow experiments

A. Genty, C. Roy, C. Geffray

- Steady-state sodium flows for Richardson's number between 0.13 and 4.2 are simulated.
- The TrioCFD code with a RANS approach and a $k - \epsilon$ turbulence model is used.
- 75% of the experimental temperature data are simulated with less than 2°C deviation.